GBT Memo #273

KFPA Measurements of the GBT Gain by Observing the Moon

Glen Langston

NRAO Green Bank

glangsto@nrao.edu

February 25, 2011

Abstract

This memo presents measurements of the GBT telescope gain and efficiency by K-band (18 to 27.5 GHz) Focal Plane Array (KFPA) observations of the Moon. These calibration observations are intended to be applied to other KFPA observations to improve absolute calibration, by correcting for errors in the reported noise diode measurements. The goal of this calibration effort is to achieve a few percent accuracy (±10%) in total intensity calibration. These observations are intended to correct the calibration values included with the GBT observations in the period September 2010 through January 2011. We applied these calibration values to the Moon observations to check the KFPA pipeline. These gain factors were checked by application to mapping observations of point sources 3C48 and 3C123, using two types of imaging convolving functions.

For observations of point sources, the mapping methods can reduce the peak intensities of point sources, by the gridding convolution process. If the image resolution is properly determined, the integrated intensities of the mapping observations are accurately measured. We find that the Moon referenced gain values yield integrated flux densities consistent with published values for 3C48 and 3C123.

Finally we comment on the accuracy of the calibration using Lunar observations, and point out priorities for improving the calibration accuracy. By improving the accuracy of models of telescope efficiency parameters, η_l and η_{mb}, absolute calibration to $\sim\pm 6\%$ is possible, based on observations of the Moon.

Change Record

Revision	Date	Author	Sections/Pages Affected
	Remarks		
1.0	2011-Feb-09	G. Langston	All
	Initial version		
1.1	2011-Feb-15	G. Langston	All
	Reduce the Scope to only TKFPA_40		
1.2	2011-Feb-20	G. Langston	All
	Revise values for fixed equations and add uncertainties		
1.3	2011-Feb-22	G. Langston	3-4
	Add description of the convolving function		
1.4	2011-Feb-23	G. Langston	All
	Detail the error estimates associated with the calibration values		
1.5	2011-Feb-23	G. Langston	2
	Fix equation array formatting		

1. Introduction

This memo presents measurements of the GBT telescope gain and efficiency by K-band (18 to 27.5 GHz) Focal Plane Array (KFPA) observations of the Moon. These calibration observations are intended to be applied to other KFPA observations to improve absolute calibration, by correcting for errors in the reported noise diode measurements. The goal of this calibration effort is to achieve a few percent accuracy ($\pm 10\%$) in total intensity calibration. These observations are intended to correct the calibration values included with the GBT observations in the period September 2010 through January 2011. We applied these calibration values to the Moon observations to check the KFPA pipeline. These gain factors were checked by application to mapping observations of point sources 3C48 and 3C123, using two types of imaging convolving functions.

The receiver noise diode values are measured in the laboratory and provided as a table of numbers by the observing system. For all observations from September 2010 through January 2011, the noise diode values measured in 2010 August 18 were provided. Later observations suggested that these values were too low, and the observations presented here are used to compute correction factors for absolute calibration.

Several authors have reported on the use of the Moon as a calibration target for large telescopes (Baars 1973; Mangum 1993; Greve et al. 1998). Observations of the Moon have a number of advantages, including large angular size, so that pointing is not an issue, and relatively high brightness temperature, so that measurement uncertainly is relatively small. The Moon has been previously observed at radio wavelengths for many years, *e. g.* Piddington & Minnett (1949), Salomonovich (1962a), Linsky (1973), and results are in good agreement.

The major disadvantage of the Moon as a calibration source are *1)* the monthly variation in average temperature and *2)* the variation in temperature with lunar latitude, as shown by Salomonovich (1962b). Radio wavelength emission from the Moon originates a few wavelengths within the surface, so shows smaller monthly variations at longer wavelengths. The lunar temperature is nearly constant at wavelengths longer than 10cm (Salomonovich 1962b).

Astronomical measurements of the brightness of radio sources can not separate two effects, *1)* uncertainty in the measurements of the Noise Diodes and *2)* overall gain of the telescope and receiver system. Fortunately, for the purposes of accurate calibration only the combination of these two factors is required.

We summarize the observations in §2 and discuss measurement of the lunar temperature in §3. In §4 we apply the deduced gain calibration values to the observations of the Moon and also to observations of bright radio source 3C48. In §5 we discuss the measured values, after calibration, from the images of the reference radio sources. In §6 the results are summarized.

For more information on the KFPA development project, see links from the page:

https://safe.nrao.edu/wiki/bin/view/Kbandfpa/WebHome

2. Observations

Observations were carried out with the GBT on 2010 December 15, as a part of KFPA commissioning tests (project TKFPA_40). On this date we measured the system response to observations of the Moon and Reference Radio source 3C48. The KFPA was used for these observations, with the IF configured in the standard manner (Langston & White 2011) and the spectrometer configured for 50MHz bandwidth centered on 23706. MHz. After pointing and focus in the standard manner, all measurements were made with the spectrometer.

The observations consisted of several components and were carried out using two astrid Scripts, `petal3C48` and `petalMoon`:

On-Off 3C48 Two spectral line scans; one On-target 3C48 and the other offset from 3C48 by 20″ in Right Ascension. The integration time was 1 second and the total observing time was 30 seconds.

Petal 3C48 A set of three Daisy (Petal) scans of 3C48, with map radius of 2.5′and radial oscillation period of 40s. The total scan duration was 80 seconds. The three Daisy scans were offset in `rotation_phase` 30^o in starting angle, to fill in the mapped region.

On-Off 3C48 Second pair of observations of 3C48, performed in the manner identical to those of the first pair.

On-Off Moon Before observations of the Moon, the IFRack input target level was set to 6. Volts, higher than the usual value of 2.5 Volts. This was intended to avoid saturation of power levels in the IF amplifier and fiber modem components. After balancing the input levels to the IFRack and spectrometer, no further gain/attenuator changes were made during this observation. The off position was located 1 degree in Azimuth relative to the Moon center position.

Petal Moon Three Daisy scans were run with radius of 17′, radial oscillation period of 120 seconds and a duration of 240 seconds. As for 3C48, the three Daisy scans were offset in `rotation_phase` 30^o in starting angle, to fill in the mapped region.

On-Off Moon A pair of scans, On and offset of the Moon center location, as was done for the first pair of On-Off Moon scans.

On the following date, 2010 December 16, we also observed bright radio source 3C123 (project TKFPA_41). Source 3C123 was mapped in the same manner as was done for 3C48; three daisy scans bracketed by On/Off source observations. The gain values are applied to these observations as well.

3. Measurements

Accurate calibration of radio wavelength observations is complicated by the number of different contributions to the observed system temperature. The calibration process is the technique by which these contributions are estimated. The measured source temperature T_{sig} values are scaled by a variety of factors, based on a model for the telescope performance and atmospheric opacity. Typically the observer will schedule an observation of empty sky, and measure the reference temperature, $T_{ref}(\nu)$, of that location.

We use a model to estimate the true brightness temperature of the moon, T_{moon}, then model the factors which reduce the measured intensity, $T_{moon,obs}$. The different effects reduce the true moon brightness temperature to the expected brightness temperature. These factors are itemized below:

Main Beam Gain The main beam efficiency, η_{mb}, must be included to determine the expected signal strength. This value is modeled, not measured. Recently Maddelena (2010) reviewed the estimates for this value, and pointed out that this factor depends on the design of the telescope optics. This parameter is particularly sensitive to the "taper" of the feed horns. This parameter is also dependent on the frequency of the observation. We estimate the uncertainty of this parameter at ±3%. A detailed study of the uncertainty of this parameter is needed.

Gain versus Elevation In addition to the main be efficiency, there is also a weak dependence of gain on elevation, $Gain(el)$. The $Gain(el)$ factor is near unity for higher elevations. The uncertainty appears to be better than ±1%. The GBT Pipeline position-switched reference Langston (2011) lists the parameters used in the calibration. To reduce the number of factors in equations 1-6, we define $\eta_{mb}(\nu, el) \equiv \eta_{mb}(\nu) \times Gain(el)$.

Rear Spillover The Ohmoic loss and rear spillover factor, η_l=0.99, reduces the measured signal strength. This parameter has never been measured for the GBT, but is expected to be accurate to better than ±1%.

Number of atmospheres The number of atmospheres, $X_{atm}(el)$, of opacity is calculated from the standard model. This parameter is well determined for $el > 10^o$.

Atmospheric Opacity The zenith opacity, $\tau_{zenith}(\nu)$, is read from a weather database. Using the source elevation at the time of the observation, the total opacity factor is calculated ($e.\ g. \tau(\nu, el) = \tau_{zenith}(\nu) \times X_{atm}(el)$). For good weather observations, the time variation is small and the factor may be estimated to better than ±0.5%. The zenith opacity was low on this day, 0.030±0.003 at 23.7 GHz, based on the archived weather measurements. We estimate the uncertainty in the opacity value by differencing the zenith opacity at the time of the observation with opacities from one hour before and after the observations. We take these larger of these two differences in opacity values as the 1σ uncertainty in the τ_{zenith}. We do not include a model for any systematic errors in τ_{zenith}. For a more detailed description of the

Table 1: Lunar Equatorial Temperatures at the time of observations on 2010 December 15

Scan	Time	Lunar phase	Lunar Temp.	el	Opacity $\tau(\nu, el)$	Opacity Scale $(1 - e^{-\tau(\nu,el)})$	$\eta_{mb}(\nu, el)$	Lunar Pred.
	(hh:mm:ss)	(deg)	(K)	(deg)				(K)
(1)	(2)	(3)	(4)	(5)	(6)	(7)	(8)	(9)
25	20:59:32	115.12	230±10	33.3	0.055±0.006	0.946±0.005	0.815±0.024	173±8
30	21:15:54	115.25	230±10	36.3	0.051±0.005	0.951±0.005	0.818±0.025	175±8

method for recording weather information see Lockman & Maddelena (2010) and references therein. Table 1 lists values of opacity used for calibration of the lunar observations.

Off Temperature The location of the off source position is assumed to have no radio sources and the only astronomical contribution assumed to the Off-source intensity is the cosmic background temperature, T_{cmb}. Assuming no pathological case of a very bright radio source in the Off position, the off temperature is accurate to the confusion limit, approximately $\sim$0.2 K, at 24 GHz. This parameter can dominate the uncertainty for observations of weak sources. By mapping the region around a source, the uncertainty in this parameter can be reduced. The 3C48 and 3C123 observations, presented here, reduce this uncertainty by fitting a model to the background brightness variation.

Ambient Temperature The contribution of Rear Spillover to the measured temperatures is the factor of Ambient Temperature, T_{amb} times the factor $(1 - \eta_l)$. The ambient temperature is measured with relatively high accuracy, typically $\pm$5 K for ambient temperatures in the range of 270 to 300 K. Also, as equation 6 shows, only the *variation* in ambient temperature adversely effects calibration.

The measured values are modeled as the sum of a several components, listed in equations (1) and

(2), which are based on equation 8.2 of *Tools of Radio Astronomy*, by Rohls and Wilson (2005). [1]

$$T_{sig}(\nu, el_1) = T_{rx}(\nu) + (T_{moon}\ \eta_{mb}(\nu, el_1) + T_{atm}(\nu))\ \eta_l \left(1 - e^{-\tau(\nu, el_1)}\right) + T_{amb}\,(1 - \eta_l) \quad (1)$$

$$T_{ref}(\nu, el_2) = T_{rx}(\nu) + (\eta_{mb}(\nu, el_2)\ T_{cmb} + T_{atm}(\nu))\ \eta_l \left(1 - e^{-\tau(\nu, el_2)}\right) + T_{amb}\,(1 - \eta_l) \quad (2)$$

$$\begin{aligned}
T_{moon,obs}&(\nu, el_1, el_2) \\
&= T_{sig}(\nu, el_1) - T_{ref}(\nu, el_2) && (3)\\
&= (T_{moon}\ \eta_{mb}(\nu, el_1) + T_{atm}(\nu))\ \eta_l \left(1 - e^{-\tau(\nu, el_1)}\right) - \\
&\quad (T_{cmb} + T_{atm}(\nu))\ \eta_l \left(1 - e^{-\tau(\nu, el_2)}\right) && (4)\\
&= \eta_l \left\{(T_{moon}\ \eta_{mb}(\nu, el_1) + T_{atm}(\nu))\ \left(1 - e^{-\tau(\nu, el_1)}\right) - \right.\\
&\quad \left.(T_{cmb} + T_{atm}(\nu))\ \left(1 - e^{-\tau(\nu, el_2)}\right)\right\} && (5)\\
&= \eta_l \left\{T_{moon}\ \eta_{mb}(\nu, el_1)\ \left(1 - e^{-\tau(\nu, el_1)}\right) - \right.\\
&\quad \eta_{mb}(\nu, el_2)\ T_{cmb}\ \left(1 - e^{-\tau(\nu, el_2)}\right) + \\
&\quad \left. T_{atm}(\nu) \left(e^{-\tau(\nu, el_2)} - e^{-\tau(\nu, el_1)}\right)\right\} && (6)
\end{aligned}$$

The cosmic background temperature, T_{cmb}, is ~ 2.725 K, and the average atmospheric temperature, $T_{atm}(\nu)$, depends on the weather. The contribution to the system temperature depends on the opacity, which is strongly dependent on elevation. The receiver temperature, $T_{rx}(\nu)$, is measured in the laboratory and is independent of weather and elevation. The ambient temperature, T_{amb}, is measured by the weather station.

The lunar brightness temperatures are measured twice at each epoch. The measured values for each of the beams is listed in Table 2. Notice the small differences in measured temperatures, indicating that measurement error is not a major contribution to overall uncertainty.

3.1. Gain Compression

During data reduction of the On- and Off-Moon observations we found that the the measured noise diode Cal-On - Cal-Off values were reduced by a small factor when observing the Moon. This calibration scale difference results in the Off-Moon noise diode calibration yielding a higher measured temperature, than measured when using the On-Moon noise diode differences. This effect is shown in Figures 1 and 2, for beam 1, Left and Right circular polarizations. The noise diode values are larger for scans 26 and 31, Off-Moon position, light and dark blue curves, respectively,

[1] The equations are from the KFPA Position Switched Calibration Plan, by Langston (2011) https://safe.nrao.edu/wiki/bin/view/Kbandfpa/PsCalibrationPlan

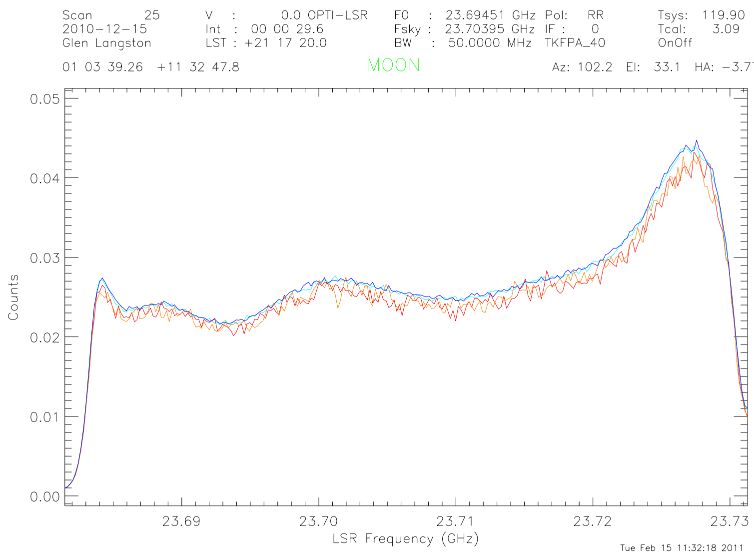

Fig. 1.— Comparison of RR polarization measured values of Cal On-Cal Off data for scans towards the Moon and offset from the Moon. Scan 25, toward Moon is red and scan 26, offset from Moon is light blue. Scan 30, toward Moon is orange and scan 31, offset from the Moon is dark blue. Notice the Cal On-Cal Off values are consistent with target location, but do not appear to be varying with time. The data are hanning smoothed and decimated to increase the SNR.

compared to the On-Moon scans 25 and 30, red and orange respectively. The scale factor difference is small, 4%, but significant. The calculations of gain factors, described in the next sections, use appropriate scaling factors, so that scale factors are appropriate for use in calibration of observations of weaker sources.

This noise diode compression effect was first noticed as a difference in the measured temperature of the moon when comparing the results of a difference in measuring the system temperature in two offset positions, compared with the results of $T_{ref}(sig - ref)/ref$ calibration. In this calibration technique, the noise diode values measured in the On-Moon position are not used.

The measured noise diode differences are consistent with position on the sky, suggesting the gain differences are not due to time variation. For measurement of the brightness temperature of the Moon, we use the On-Moon measured counts of noise diode intensity. For the Off-Moon measurements, we use the Off-Moon noise diode values, to compensate for gain compression.

4. Gain Calibration

The gain calibration process has three major parts, *1)* estimating the Moon brightness temperature, *2)* computing the antenna gain factors and *3)* application of these factors to imaging observations.

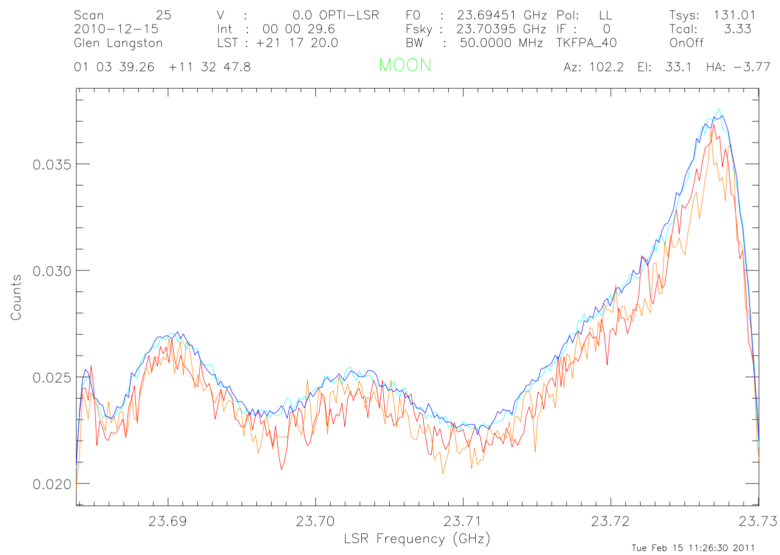

Fig. 2.— Comparison of LL polarization measured values of Cal On-Cal Off data for scans towards the Moon and offset from the Moon. This plot is zoomed in on the central range of the values, compared to the full range shown in the previous figure. The color coding is the same as in the previous figure.

After application of the gain factors, we checked the accuracy of the factors by measuring the flux density of sources 3C48 and 3C123.

4.1. Moon Brightness Temperature

Linsky (1973) proposed use of the Moon as a Radiometric standard for microwave calibration of large radio telescopes. They proposed that the average of all measurements of one lunar month, 29.53 days, be used the standard. They made a complete set of observations at many wavelengths, from 12μm to 1m. We adopt the lunar center brightness temperature average value of 239$\pm$10 K from Linsky (1973) for 1.25 cm (24.0 GHz).

Salomonovich (1962a) tabulated a large number of Moon temperature measurements at different wavelengths. These observations show a phase offset between lunar phase and peak brightness temperature. Figure 3 shows their observations at 0.88 cm for 4 different lunar phases.

Assuming a sinusoidal variation of temperature as a function of lunar phase, with a phase offset, we model the physical temperature as a function of date. New Moon corresponds to a phase of 0^o and full Moon phase is 180^o. The phase offset is 40 ± 5 deg and amplitude is 35$\pm$5 K. We apply this model to estimate the lunar brightness temperature at the time of the observations, listed in Table 1. For this date the lunar phase was 115.1^o and the lunar temperature was T_{moon} =230.0$\pm$10.1

K. The relative temperature uncertainty was 4.4%. After computation of all gain factors for all beams and polarizations, these values are tabulated and input to the KFPA pipeline for use in all subsequent calibrations of KFPA data.

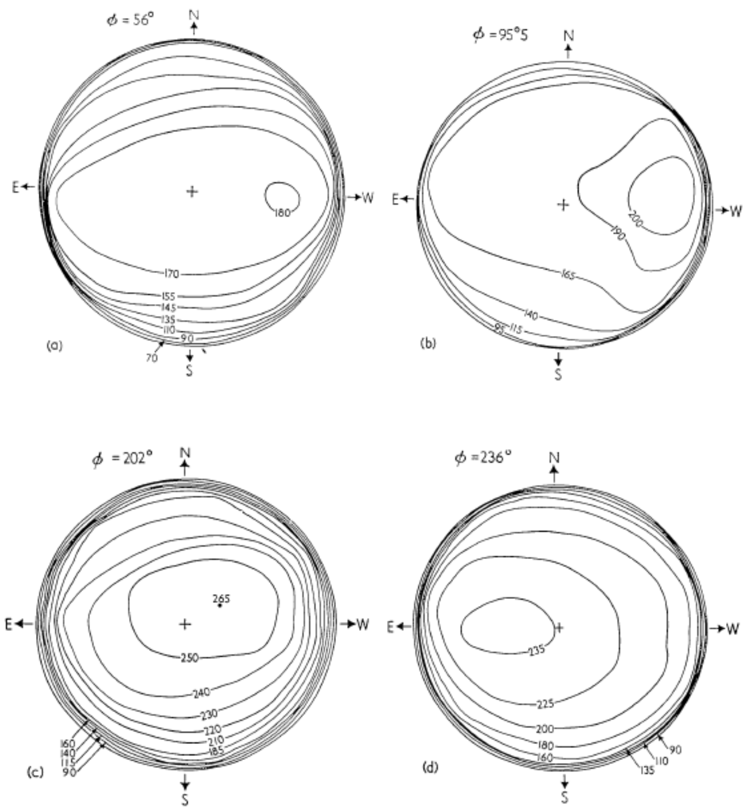

Fig. 3.— Images of the Moon taken at 8mm (37.5 GHz) at different lunar phases by Salomonovich (1962b).

4.2. Computing Gain Factors

We computed the gain correction factors by modeling the predicted Moon brightness temperature, using equation 6, above. The values used for this calculation for the two Moon observations are listed in Table 1. Column (9) of Table 1 is the predicted value of Lunar Brightness temperature that would be expected, assuming the opacity and gain model described by equations 1-6.

$$Gain_{beam,polarization} = T_{moon}/T_{moon,obs,beam,polarization} \qquad (7)$$

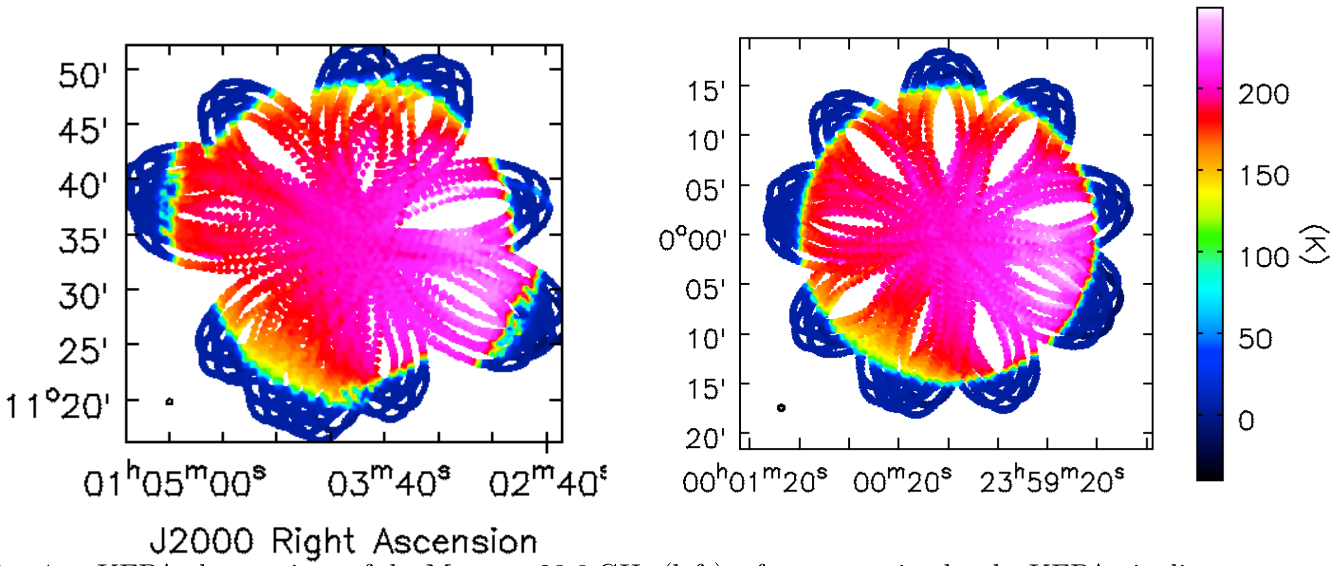

Fig. 4.— KFPA observations of the Moon at 23.8 GHz (left), after processing by the KFPA pipeline. On the right are the same data, after translation of coordinates to a moon centered frame. The temperature of the center of the moon is the calibration reference signal, T_{moon}. Note that the sub-solar point, to the right, is significantly hotter and that the lunar poles, upper right and lower left, are significantly colder.

In Table 2, we list the observed differences in antenna temperature between On-Moon and Off-moon observations. Next we computed the ratio of the expected temperature to the measured temperature independently for each of the two observations. These values are shown in Table 3. One value is measured for each beam and polarization. On this date, an amplifier for beam 4, Left circular polarization had failed, so no values are available. Finally we average the two gain factors to determine the calibration factors. Also we difference the two values to estimate the 1σ uncertainty in the calibration factors. These measurement uncertainties are generally smaller than $\pm 1\%$. We discuss the systematic uncertainties in later sections.

The anomalously high difference in two measurements for beam 4, right circular polarization value, may be due to gain instabilities for this beam.

The average gain factor values, in Table 3, should be applied to all observations made during the interval from September 2010 through January 2011.

4.3. Image of the Moon

Results of the pipeline calibration and imaging are shown in Figure 4-a and 4-b. Figure 4-a shows the observations in the RA-Dec frame. During the observations, the Moon is steadily moving. Bob Garwood provided some GBTIDL scripts which take as arguments the calibrated spectra files, the raw observation spectra and two scan numbers. The scan numbers correspond to two observations when tracking the center of the Moon. The procedures interpolate in time the coordinate offsets and apply these offsets to the image spectra. These scripts work with any GBT observations made toward moving bodies (Moon, planets or comets). The result of this computation is show in Figure 4-b.

Mapping observations consisted of 3 Daisy scans with radius of $17'$ and scan period of 120 seconds. The 3 scans have starting orientations offset by 30^o to provide more uniform coverage of the object in a short duration. These Moon map scans required 12 minutes observation. A full Daisy pattern would require 23 motions of 120s duration, or 46 minutes.

Figure 4-b shows that the temperature variation in the center of the Moon is small, while the lunar poles show significantly lower temperature. The sub-solar point on the Moon shows a significantly higher temperature. This effect is included in the temperature model.

4.4. Application to 3C48 and 3C123

After computing the gain factors, these factors they were applied to observations of source 3C48. The pipeline was run with the '–allmaps' argument, which creates images of all images in an observing session. The pipeline also provides the spectra calibrated in a variety of ways, for the 3C48 observation the calibration was in Janskys (pipeline argument '-u Jy'). The 3C48 observations were carried out using the pipeline without tuning any special parameters for calibration and imaging. The default image gridding method for the pipeline is using a Gaussian convolution function. This method produces a smoother output image, with fewer extrema than the alternate sync-Bessel convolution function.

As noted, the 3C48 image was produced from 3 Daisy scans of the region which were position-switch calibrated in the standard manner. The resulting image is shown in Figure 5. The image of 3C123 is show in Figure 7. The pipeline input file is shown in Figure 7.

4.5. Convolving Functions

After calibration, the KFPA pipeline performs imaging using AIPS single dish tools. These tools have a number of options, including the number of channels to average, image size, pixel size and convolving function parameters.

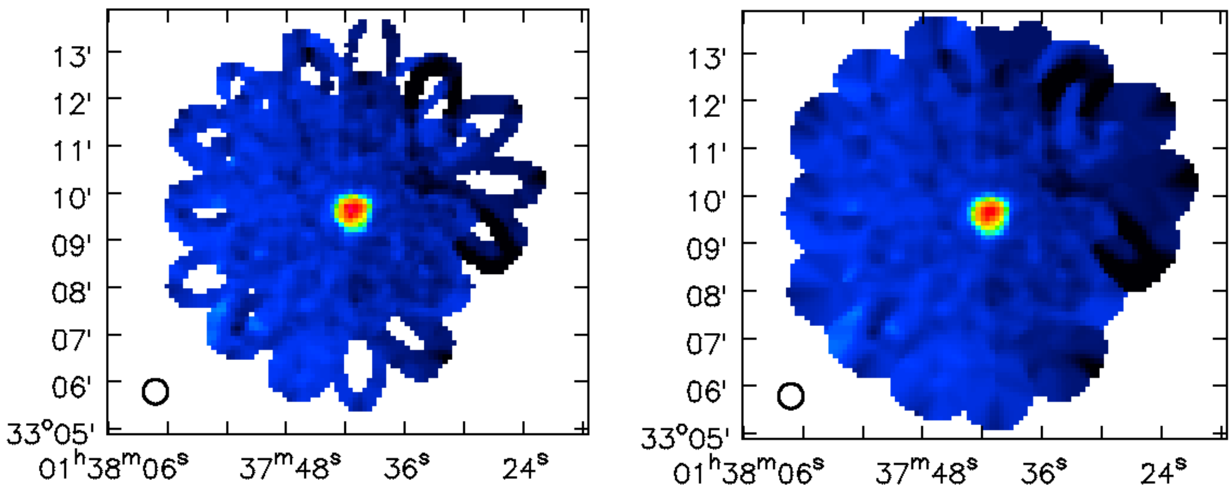

Fig. 5.— KFPA image of 3C48 after calibration and convolving samples with a Sync-Bessel function (left). The convolving function diameter is 3 pixels. The color scale range is -0.3 to 0.9 Jy/Beam. KFPA image of 3C48 after convolving with a Gaussian function (right). The convolving function FWHM is 9″ and the function diameter is 5 pixels.

Since the GBT spectral integrations are made while moving the telescope at a rate of approximately 4 samples per FWHM beam width, there is a slight smearing of the source by approximately ∼8″ in the along-motion direction. Also since the pixels approximately 1/5th of the beam size, this results an image with slightly reduced angular resolution. This effect is sean in the resulting 3C48 images. Note that the total flux density is conserved, but is smeared. By accounting for the GBT angular resolution in the imaging process, a point source flux density is recovered in the measurement of the integrated intensity.

The convolving function parameters determine how the irregularly sampled spectra are placed on the square grid of image pixels. The convolving function is intended to smooth data and interpolate between spectra taken at slightly offset locations. There are two types of convolving functions used with the pipeline, a Gaussian convolving function and a sync-Bessel convolving function. The Gaussian function has the advantage of smoothly interpolating between sampled spectra, with the disadvantage of a slight loss of angular resolution. The imaging parameters for the pipeline are the result of a number of experiments with different parameters. For the KFPA, we found that visually appealing images if relatively small pixel sizes were used. For observations at 23706 MHz, the average of the NH_3 1,1 and 2,2 transitions, 6″ square pixels were a good choice for the 31.3″ GBT FWHM beam width. This pixel size results in a FWHM beam width of ∼5 pixels. The AIPS task SDGRD takes as an argument the number of pixels in the convolving function. For the

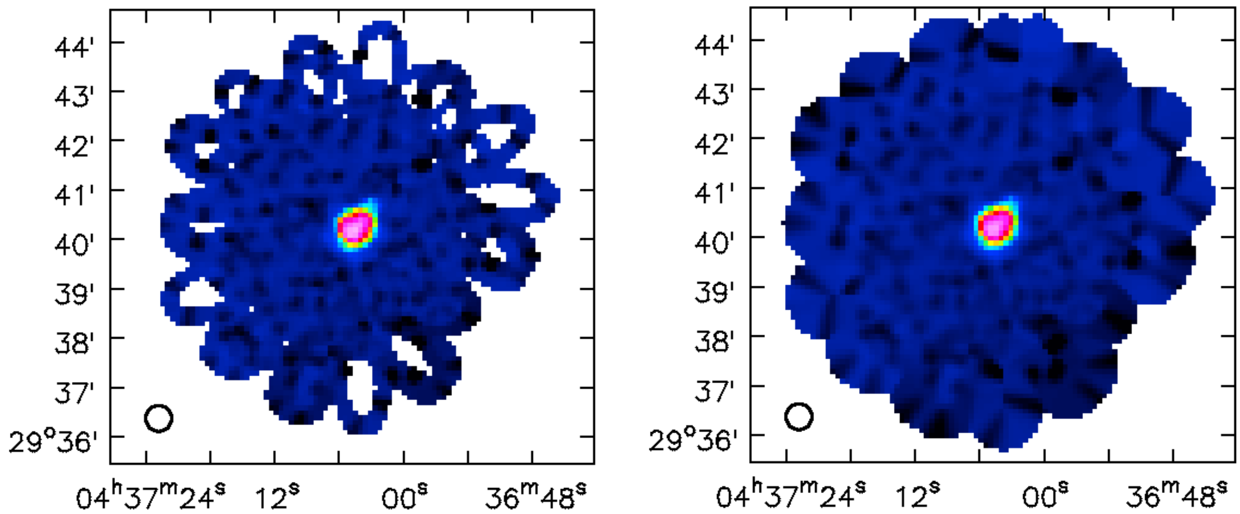

Fig. 6.— KFPA image of 3C123 after calibration and convolving samples with a Sync-Bessel function (left). The convolving function diameter is 3 pixels. The color scale range is -0.3 to 1.7 Jy/Beam. KFPA image of 3C123 after convolving with a Gaussian function (right). The convolving function FWHM is 9″ and the function diameter is 5 pixels.

Gaussian function, a 5 pixel diameter convolving function is appropriate. Since the sky is sampled roughly every 9″, this was chosen as the Gaussian FWHM. Convolving the GBT beam size with a 9″ Gaussian yields an image angular resolution of 32.6″.

If slightly higher angular resolution is required in the GBT image, the Sync-Bessel convolving function may be used. As described by Mangum et al. (2007), this yields higher angular resolution at the cost of sightly noisier image, with reduced ability to interpolate between gaps in the spectral samples. Note that the Sync-Bessel convolution function is negative at larger angular distances from the sample location. In order to avoid numerical problems, we limited the convolving function diameter to 3 pixels. Otherwise our convolving function parameters are the same as those used by Mangum et al. (2007). Since the minimum convolving function is the pixel size, 6″, the resulting angular resolution of the image was was 31.8″. Integrating the 3C48 intensity yields the expected source brightness, within the uncertainty of the measurement. See Figure 4 and Table 4.

Note that the peak intensity of the point sources are reduced in the images, due to smearing the source by observing while moving the GBT pointing direction. Slowing the telescope motion and decreasing the angular separation of adjacent scans of the source will reduce the source smearing. The image contains all of the source emission, and by properly accounting for the image angular resolution, the total flux density is measured.

4.6. Fitting Intensity Model

After imaging the region, the spectral line cube summed to produce a continuum image. We chose to reduce the spectral resolution to 6.1 MHz and fit the source sizes using the central channel of the band. The fit to the image was accomplished with AIPS task JMFIT. The model continuum intensity image consisted of two components. Component 1 was a two dimensional gaussian of the source intensity. Component 2 was a continuum model (plane) of the background brightness variation. (The JMFIT arguments are `CTYPE = 1, 3, 0 ; DOPOS=1 ; DOWID=1 ; DOMAX = 1; NITER = 1000 ; NGAUS = 2.`)

Component 1 measures the source intensity and also source smoothing due to observations while moving the telescope. The resulting component fit shows the angular resolution of the observation was 37.3±2.8 × 35.1±2.7 with postion angle $\theta = 120 \pm 50^o$.

Component 2, the background intensity measures the un-modeled sky brightness variation and any un-modeled galactic background intensity. For this observation, the background was slightly negative, with average intensity of -0.1 Jy.

Table 4 lists the flux densities available from Baars et al. (1977) and Ott et al. (1994) for 3C48 and 3C123, along with values deduced from these measurements, after application of the gain factors. Note that the measurement uncertainty is relatively large for the estimate of the total intensities of these sources. By reducing the mapping speed, the flux densities could be more accurately measured.

Table 5 presents the positions and angular sizes of the Gaussian fit to the point source images. The source positions are very close to the published values, within $\pm 2.0''$, which is better than might be expected due to the overall uncertainty in the GBT pointing accuracy. This small offset may be due to the fact that these sources were used to determine the local pointing corrections just before the start of mapping observations.

Figures 5 and 6 show images of 3C48 and 3C123 produced with "Sync-Bessel" and "Gaussian" convolving functions. Table 5 also shows the source size resulting from the intrinsic GBT angular resolution, the motion of the telescope while sampling the sky brightness and the convolution of the spectral samples onto the image grid. Source 3C48 has a very small angular size, $< 3''$. Source 3C123 has a bright core component at 22 GHz, and fainter extended emission out to $\sim 30''$ (Looney & Hardcastle 2000). The fainter extended emission is detected in the GBT images.

5. Results

On-Off Observations of the Moon were used to compute the beam/polarization scaling factors needed to calibrated the KFPA mapping intensity scale. The application of these factors in the KFPA pipeline results in measured values of the intensities of bright reference radio sources 3C48 and 3C123 that are consistent with published values to within 10%.

The calibration accuracy based on Moon observations is limited the following factors:

Lunar Brightness Uncertainty is limited by methods of calibration of other radio telescope observations. The reported accuracy of other observers measurements have an uncertainty of 10.1K for a lunar temperature of 230.K, or a 4.4 % uncertainty.

$\eta_{mb}(\nu, el)$ The uncertainty in the main beam efficiency is approximately 3%. Reducing this uncertainty is a priority for reducing the absolute uncertainty of lunar calibration.

Measurement The measurement uncertainties, based on repeated observations, suggest that the lunar brightness can be measured to ± 2 %.

Opacity The opacity scale factor uncertainty is relatively small in good weather, approximately $\pm 1\%$.

Linearity The Moon antenna temperature is higher than normally encountered in astronomical observations. Gain compression can compromise the measurement accuracy. Measurement accuracy of $\pm 1\%$ should be achievable.

Assuming all these uncertainties add in quadrature, the resulting accuracy of the calibration factors based on the Lunar Observations is $\pm 6\%$. This accuracy exceeds the calibration accuracy obtainable from published flux densities of bright compact reference radio sources.

These calibration factors, given in Table 3, should be applied to all KFPA commissioning and shared risk observations from the interval September 2010 to January 2011.

Additional observations are needed for more reference radio sources, mapping at a slower angular rate, to reduce the measurement uncertainty. After each major change to the KFPA, the Moon calibration observations should be repeated to confirm the noise diode calibration values.

REFERENCES

Baars, J. W. M. 1973, IEEE Transactions on Antennas and Propagation, 21, 461

Baars, J. W. M., Genzel, R., Pauliny-Toth, I. I. K., & Witzel, A. 1977, A&A, 61, 99

Greve, A., Kramer, C., & Wild, W. 1998, A&AS, 133, 271

Langston, G. I. 2011, *GBT Memo Series*, 274

Langston, G. I., & White, S. 2011, GBT Memo Series, 275

Linsky, J. L. 1973, ApJS, 25, 163

Lockman, F. J., & Maddelena, R. J. 2010, *GBT Memo Series*, 267

Looney, L. W., & Hardcastle, M. J. 2000, ApJ, 534, 172

Maddelena, R. J. 2010, *GBT Memo Series*

Mangum, J. G. 1993, PASP, 105, 117

Mangum, J. G., Emerson, D. T., & Greisen, E. W. 2007, A&A, 474, 679. 0709.0553

Ott, M., Witzel, A., Quirrenbach, A., Krichbaum, T. P., Standke, K. J., Schalinski, C. J., & Hummel, C. A. 1994, A&A, 284, 331

Piddington, J. H., & Minnett, H. C. 1949, Australian Journal of Scientific Research A Physical Sciences, 2, 63

Salomonovich, A. E. 1962a, Soviet Ast., 6, 55

— 1962b, in The Moon, edited by Z. Kopal & Z. K. Mikhailov, vol. 14 of IAU Symposium, 491

Table 2. Measured Lunar Temperatures

Scan	1 L (K)	1 R (K)	2 L (K)	2 R (K)	3 L (K)	3 R (K)	4 L (K)	4 R (K)	5 L (K)	5 R (K)	6 L (K)	6 R (K)	7 L (K)	7 R (K)
25	95.5	86.5	98.7	94.0	88.9	89.1	90.0	-	78.5	79.8	80.6	81.0	68.5	70.8
30	96.2	86.7	99.4	94.9	88.8	89.6	94.9	-	79.0	80.7	81.1	81.2	69.3	71.4

Table 3. Scale Factors deduced from Lunar Temperatures

Scan	1 L	1 R	2 L	2 R	3 L	3 R	4 L	4 R	5 L	5 R	6 L	6 R	7 L	7 R
25	1.812	2.001	1.754	1.841	1.947	1.943	1.923	-	2.205	2.169	2.147	2.137	2.527	2.445
30	1.817	2.016	1.758	1.842	1.968	1.951	1.842	-	2.212	2.166	2.151	2.152	2.522	2.448
Ave.	1.815	2.008	1.756	1.842	1.958	1.947	1.882	-	2.209	2.167	2.145	2.145	2.524	2.446
$\pm$	0.004	0.015	0.005	0.001	0.021	0.008	0.081	-	0.007	0.003	0.008	0.016	0.005	0.003

Table 4: Flux Density Measurements compared with published values

Source Name	Baars Total (Jy)	Ott Total (Jy)	Sync+Bessel Peak (Jy)	Sync+Bessel Total (Jy)	Gaussian Peak (Jy)	Gaussian Total (Jy)
3C48	1.034±0.085	1.130±0.093	0.874±0.066	1.125±0.136	0.850±0.069	1.111±0.143
3C123	-	2.925±0.293	2.001±0.062	2.931±0.140	1.957±0.065	2.862±0.146

Table 5: Source Position and Size from Fits to Different Convolution Functions

Source Name	Convolution Type	RA hh:mm:ss	Dec dd:mm:ss	Major Axis (″)	Minor Axis (″)	Position Angle (deg)
3C48	Sync+Bessel	01:37:41.32±0.09	33:09:37.4±1.2	37.3±2.8	35.1±2.7	121±50
3C48	Gaussian	01:37:41.34±0.10	33:09:37.3±1.3	38.3±3.1	36.2±2.9	121±60
3C48	Published	01:37:41.30	33:09:35.4	<3		
3C123	Sync+Bessel	04:37:04.46±0.04	29:40:15.2±0.5	46.7±1.3	34.9±1.1	136±6
3C123	Gaussian	04:37:04.47±0.04	29:40:15.1±0.6	43.1±1.4	36.0±1.2	136±7
3C123	Published	04:37:04.40	29:40:15.0	<30		

```
#KFPA pipeline arguments for point source 3c123
--clobber
-v 4
--refscan1 22
--refscan2 27
#potentially turn off automatic mapping
--imaging-off
#--allmaps
-m 23:25
#Limit noise range to 4 K RMS
-n 4.0
#The following allows selecting all beams, but 4
#-f 1,2,3,5,6,7
#-f -4
#Potentially select only RR or LL polarization
#-p RR
#Select the maximum number of processors
#--max-processors 14
--gain-factors-left  1.815,1.756,1.958,1.882,2.209,2.151,2.524
--gain-factors-right 2.008,1.842,1.947,1.900,2.167,2.145,2.446
-i /home/sdfits/TKFPA_41/TKFPA_41.raw.acs.fits
#-u Tmb
-u Jy
```

Fig. 7.— KFPA Pipeline arguments to calibrate observations of 3C123